# Comparative Direct Analysis of Type Ia Supernova Spectra. II. Maximum Light

David Branch[1], Leeann Chau Dang[1,2], Nicholas Hall[1], Wesley Ketchum[1], Mercy Melakayil[1], Jerod Parrent[1], M. A. Troxel[1], D. Casebeer[1], David J. Jeffery[1], & E. Baron[1]

## ABSTRACT

A comparative study of near–maximum–light optical spectra of 24 Type Ia supernovae (SNe Ia) is presented. The spectra are quantified in two ways, and assigned to four groups. Seven "core–normal" SNe Ia have very similar spectra, except for strong high–velocity Ca II absorption in SN 2001el. Seven SNe Ia are assigned to a "broad–line" group, the most extreme of which is SN 1984A. Five SNe Ia, including SN 1991bg, are assigned to a "cool" group. Five SNe Ia, including SN 1991T, are assigned to a "shallow–silicon" group. Comparisons with **Synow** synthetic spectra provide a basis for discussion of line identifications, and an internally consistent quantification of the maximum–light spectroscopic diversity among SNe Ia. The extent to which SN Ia maximum–light spectra appear to have a continuous distribution of properties, rather than consisting of discrete subtypes, is discussed.

*Subject headings:* supernovae: general

## 1. INTRODUCTION

In the first paper of this series (Branch et al. 2005; hereafter Paper I), the parameterized supernova synthetic–spectrum code **Synow** was used to fit and interpret a time series of spectra of the well–observed, spectroscopically normal, Type Ia (SN Ia) SN 1994D. In this paper we concentrate on near–maximum–light spectra of 24 SNe Ia. Maximum–light spectra are of particular interest because they are the ones most likely to be obtained, especially for high–redshift SNe Ia. In §2 the spectra are quantified and arranged to illustrate relationships

[1]Homer L. Dodge Department of Physics and Astronomy, University of Oklahoma, Norman, OK 73019; e-mail: branch@nhn.ou.edu

[2]Department of Astronomy, Whitman College, Walla Walla, WA 99362

between them. In §3 to §6 four groups of spectra are discussed, and selected comparisons with **Synow** synthetic spectra are shown. Results are discussed in §7.

As in Paper I, we confine our attention to optical spectra, from the Ca II H&K feature in the blue ($\sim$ 3700 Å) to the Ca II infrared triplet (Ca II IR3) in the red ($\sim$ 9000 Å). The 24 spectra selected for study were obtained within three days of $B$–band maximum light [which occurs about 18 days after explosion (Vacca & Leibungut (1996)], a time interval short enough that spectroscopic evolution is not strong, yet long enough to allow some events of special interest to be included. All spectra have been corrected for the redshifts of the parent galaxies. The original spectra have a range of slopes, owing to intrinsic differences, differences in the amount of reddening by interstellar dust, and observational error. In this paper, because we are interested only in the spectral features, and not in the underlying continuum slopes, the spectra are tilted by multiplying the flux by $\lambda^{\alpha}$, with $\alpha$ chosen to make the flux peaks near 4600 Å and 6300 Å equally high. The tilting makes it much easier to compare the spectral features. The events of the sample are listed in Table 1, together with parameters to be discussed below.

## 2. ARRANGING THE SPECTRA

Various ways of arranging the spectra according to measurements of selected features were explored. The arrangement shown in Figure 1 appears to be useful. The $W(5750)$ parameter is the equivalent width of the absorption near 5750 Å, usually attributed to Si II $\lambda$5972, and $W(6100)$ is that of the stronger absorption near 6100 Å, produced by Si II $\lambda$6355. (Because of the presence of emission features, these are equivalent–width–*like* quantities rather than true equivalent widths.) The wavelength limits of integration are chosen by eye[1] in the same way as they are for measuring the $R$(Si II) parameter, which is the ratio of the fractional depths of these two absorptions (Nugent et al. 1995), and the flux used as the divisor of the intregral is the mean of the fluxes at the wavelength limits. The ratio of $W(5750)$ to $W(6100)$ is correlated with, but not equal to, $R$(Si II). For our present purpose of arranging the spectra, the measurement errors are not important, even though the fractional error of $W(5750)$ is large when $W(5750)$ is small.

Plotting $W(5750)$ against $W(6100)$ illustrates the relationships according to only two spectral features. To quantify the relationships over a broader wavelength range, the spectra were interpolated onto a standard wavelength grid of 2 Å separation, and for each pair of

[1]A precisely defined method, such as used by S. Bongard et al. (in preparation) will be required when strictly reproducible results are needed.

spectra the $\chi^2$–like figure of merit formed from the logarithmic flux differences between 3700 and 6500 Å (or as much of this interval as possible) was minimized by scaling the flux and varying the tilt (Appendix A). The results identify the nearest neighbor of each event. In Figure 1, a single–headed arrow points to a nearest neighbor (e.g., SN 2002bf is the nearest neighbor of SN 1984A) and a double–headed arrow connects events that are mutual nearest neighbors.

In §3 to §6 four groups of spectra, denoted by different symbols in Figure 1, are considered. The group assignments were made on the basis of Figure 1, as well as on the appearance (depth, width, and shape) of the 6100 Å absorption feature. Some comparisons with synthetic spectra are shown, and line identifications are discussed.

## 3. CORE–NORMALS

Figure 2 shows spectra of seven SNe Ia that are tightly clustered in Figure 1 and have similar 6100 Å absorptions, not only in equivalent width but also in shape. Other features, even weak ones, also are similar. These will be referred to as "core–normal" SNe Ia. The only conspicuous difference among them is the strong high–velocity Ca II IR3 absorption near 8000 Å in SN 2001el.

In Branch et al. (2003) and in Paper I, **Synow** fits to the spectra of two core–normals, SN 1998aq and SN 1994D, were presented and discussed. Descriptions of the **Synow** code and its use can be found in these two papers and references therein. For the present work, we adopted precepts for fitting spectra of core–normals that differ mildly from those of previous papers. For photospheric–velocity (PV) ions the line optical depth $e$–folding velocity, $v_{\rm e}$, is 1000 km s$^{-1}$. For most detached high–velocity (HV) ions, $v_{\rm e}$ = 2000 km s$^{-1}$. (HV Ca II in SN 2001el is an exception.) The excitation temperature, $T_{\rm exc}$, is 10,000 K. The ions used are PV O I, Mg II, Si II, Si III, S II, Ca II, Fe III, Co II, and Ni II, HV Ca II, and HV Fe II. In Paper I, Na I also was used, but the identification (at maximum light) was not considered to be definite. In this paper Na I is not used for core–normals, on the grounds that if Na I were present in core–normals then it should be much stronger in cooler SN 1991bg–like events, which is not the case. Lines of C II also are not used, because if present at maximum light they are weak and difficult to confirm [although they appear to be present at maximum light in at least SN 1998aq (Branch et al. 2003), and will be used in Paper III (in preparation) on premaximum–light spectra]. In Paper I, HV Fe II was not used in near–maximum–light spectra. In this paper HV Fe II is used[2] because we now have stronger evidence for its

[2]In the course of this work the Fe II log $gf$ values of the Kurucz (1993) line list, on which **Synow** relies,

presence, as discussed below. The **Synow** fitting parameters for the core–normals are listed in Table 2.

In Figure 3 the spectrum of SN 1994D is compared with two synthetic spectra. As usual, the blackbody continuum of **Synow** makes the synthetic spectrum too high from about 6500 Å to 7800 Å. (The continuum of SNe Ia cannot be modeled as a single blackbody curve, but an attempt to model the exact continuum shape at the **Synow** level of analysis would be an unrewarding fitting exercise.) One synthetic spectrum includes HV Fe II, detached at 16,000 km s$^{-1}$, and the other does not. The main effect of HV Fe II is produced by two lines of multiplet 42, $\lambda$5018 and $\lambda$4924. (The third line of the multiplet, $\lambda$5169, is in this case overwhelmed by Si II absorption.) In SN 1994D and most other events of the sample, an absorption near 4430 Å, which we believe to be produced by Si III $\lambda$4550, is not well fitted because the Si III synthetic absorption is too blue. The fit could be improved by lowering $v_{\rm phot}$ and slightly detaching all ions other than Si III, but this would not help us to understand the discrepancy so we have refrained from doing it. Because the synthetic spectra usually are too high in the red, and because of the presence in some spectra of the telluric absorption near 7600 Å, it is difficult to know how to fit the absorption produced by O I $\lambda$7773 (and Mg II $\lambda$7890), so little significance should be attached to the fitting parameters used for O I.

In Figure 4 the spectrum of SN 2001el is compared with a synthetic spectrum in which HV Ca II has a high optical depth ($\tau = 12$, compared to $\tau = 2$ to 5 for other core–normals), a high value of $v_{\rm e} = 12{,}000$ km s$^{-1}$, and a maximum velocity of 30,000 km s$^{-1}$. The high value of $v_{\rm e}$ makes the absorption flat and extend to the maximum velocity. This fit is not unique, but it demonstrates that HV Ca II can account for the feature. Polarization observations indicate that asymmetry, not taken into account in **Synow**, affects HV Ca II line formation in SN 2001el (Wang et al. 2003, Kasen et al. 2003). The best fit for SN 2001el is obtained with a HV Fe II optical depth that is the highest among the core–normals. Since SN 2001el has strong HV Ca II absorption, this is regarded as support for the HV Fe II identification. The normality of all features *not* affected by HV Ca II and HV Fe II indicates that the PV spectrum of SN 2001el is very much like those of the other core–normals.

Most of the spectral features of the core–normals have established line identifications. Ions whose presence is considered to be definite are PV Si II, S II, Ca II, O I, Mg II, Fe III, and HV Ca II. Co II and Si III are probable, while Ni II is possible, but difficult to

---

were compared with those derived by Phillips (1979) from the solar spectrum. Among the strong lines two significant discrepancies were found, and the Phillips values of log $gf(\lambda5169)=-1.66$ and log $gf(\lambda4549)=-2.67$ were adopted.

establish. We will return to the issue of HV Fe II below. The issue of C II will be addressed in Paper III (in preparation) on premaximum spectra. A few of the weak features of the core–normals are not reproduced by the **Synow** spectra. Possible identifications of the weak absorptions near 5500 Å and 5150 Å (seen most clearly in Figure 3) are Si III $\lambda$5740 and Co II $\lambda$5311, respectively. The weak absorptions near 4150 Å and 4550 Å (see Figure 2) remain unidentified (but see §7 on the 4550 Å absorption).

## 4. BROAD–LINE SNe Ia

Figure 5 shows the spectrum of the core–normal SN 1994D (for comparison) and the spectra of seven SNe Ia that are spectroscopically normal in the traditional sense that their strongest spectral features are the usual ones, rather than the conspicuous Fe III features of SN 1991T or the blue Ti II trough of SN 1991bg. However, these seven "broad–line" SNe Ia have 6100 Å absorptions that are broader and deeper than those of the core–normals, which puts them to the right of the core–normals in Figure 1. The spectra of SN 1992A and SN 1981B are not very different from core–normal, but their lines are broader, e.g., notice the lack of resolution in the absorption complex from 4600 Å to 5100 Å. Therefore, we regard SN 1992A and SN 1981B as small steps from the core in the direction of SN 1984A. The spectra of Figure 5 do not appear to comprise a simple one–dimensional sequence. In SN 2002bf the absorption near 7500 Å is broad and shallow. SN 2001ay has a weak Ca II IR3 absorption and steep pieces of spectra near 4000 Å and 4200 Å. [Extreme photometric peculiarities of SN 2001ay are discussed by Howell & Nugent (2004).]

The fitting parameters for the broad–line SNe Ia are in Table 3. The ions are the same as for the core–normals. Reasonable fits were obtained with $v_{\rm phot}$ = 12,000 km s$^{-1}$, a typical value for core-normals, and higher values of $v_{\rm e}$: 2000 km s$^{-1}$ for both PV and HV ions, or higher as indicated in Table 3. For consistency with the modeling of the core–normals, PV and HV components were used for Ca II, but these broad Ca II features also can be fitted as single high–$v_{\rm e}$ components, so the Ca II fitting parameters are far from uniquely determined.

In Figure 6 the spectrum of the moderately broad–line SN 2002bo is compared with two synthetic spectra. HV Fe II, with a high optical depth of 1.5, affects the synthetic spectrum in several places. In Figure 7 SN 1984A is compared with synthetic spectra in which Si II has $v_{\rm e}$ = 5000 km s$^{-1}$ and a maximum velocity of 25,000 km s$^{-1}$. The quality of these two fits is about the same as for the core–normals.

Line identifications in the broads are the same as in the core–normals. Given the non–uniqueness of **Synow** fits (e.g., to an extent, lowering $v_{\rm e}$ can be compensated by raising the

optical depth), most of the differences between the optical depths used for the broads and the core–normals are not necessarily significant.

## 5. COOL SNe Ia

Figure 8 shows spectra of the core–normal SN 1990N and five "cool" SNe Ia, four of which have a conspicuous absorption trough from about 4000 to 4400 Å, due in part to PV Ti II (Filippenko et al. 1992a; Mazzali et al. 1997; Garnavich et al. 2004). SN 1989B, on the other hand, is spectroscopically normal in the traditional sense, and not far from core–normal, but its 6100 Å absorption is deeper than in the core–normals. Its $W(6100)$ value is similar to that of SN 1981B, which is one of the broad–line events of §4, but the features of SN 1989B are better resolved than those of SN 1981B. Notice, for example, the well resolved region between 4600 Å and 5100 Å in SN 1989B. The 6100 Å absorption of SN 1989B is almost identical to that of SN 1986G. For these reasons, we regard SN 1989B as a small step from the core in the direction of SN 1991bg–like spectra, and it is included with the cools even though it does not have the blue absorption trough.

The fitting parameters for the cool SNe Ia are in Table 4. SN 1989B can be fitted with parameters that differ only mildly from those of the core–normals. For the others of Figure 8, the PV excitation temperature is lowered from 10,000 to 7000 K in view of the development of Ti II lines, which require low temperature. In addition to Ti II, five more ions, Na I, Mg I, Ca I, Sc II, and Cr II, are introduced. Garnavich et al. (2004) used Mg I and Ca I in their study of SN 1999by, and Sc II also is plausible at low temperature. (Sc II lines appear in SNe II when they become sufficiently cool.) Si III and Fe III require high temperature so they are not used for the cools.

The spectrum of SN 1986G cannot be well fitted with the precepts that were adopted for the core–normals; when the 6100 Å absorption is fitted, the 5750 Å absorption, which is strong in the observed spectrum, hardly appears in the synthetic spectrum. A plausible solution is to impose a maximum velocity on Si II. In Figure 9 the spectrum of SN 1986G is compared with a synthetic spectrum in which Si II has a maximum velocity of 15,000 km $s^{-1}$ and a high optical depth of 100. Owing to the maximum velocity, the 6100 Å absorption saturates, and owing to the high optical depth, the 5750 Å absorption appears.

It has been suggested (Garnavich et al. 2004) that Ti II may contribute to the 5750 Å absorption in SN 1991bg–like spectra, but we find that when the Ti II optical depth is chosen to fit the blue trough, Ti II makes no significant contribution to the 5750 Å absorption. (If the Ti II optical depth is raised, or an improbably high value of $T_{\rm exc}$ is used, an absorption

due to Ti II lines does appear near, but not near enough, to the 5750 Å absorption.) On the basis of detailed spectrum calculations with the PHOENIX code (Baron et al. 2003 and references therein), S. Bongard et al. (in preparation) also conclude that Ti II makes no contribution to the 5750 Å absorption. Again, a plausible solution is to impose a maximum velocity on Si II. This is shown in Figure 10 for SN 1991bg; in the synthetic spectrum the Si II maximum velocity is 14,000 km s$^{-1}$ and the optical depth is 200.

In view of the large number of ions that may be present, line identifications in the cools (other than SN 1989B) are a challenge. Si II, Ca II, Mg II, Ca II, and Ti II can be regarded as definite. (Contrary to previous opinion, S II cannot, because Sc II has lines that could be wrongly attributed to S II.) As shown in Figures 9 and 10, Cr II, Sc II, Mg I, Ca I, Na I, Co II, and Ni II can be combined to obtain reasonable fits; all of these ions are plausible, but none are definite.

## 6. SHALLOW–SILICON SNe Ia

Figure 11 shows spectra of the core–normal SN 1994ae and five "shallow–silicon" SNe Ia that have smaller values of $W(5750)$ and $W(6100)$, thus occupying the lower left corner of Figure 1. Despite their shallow Si II absorptions, SN 1999ee and SN 1999aw are spectroscopically normal in the traditional sense. SN 1991T and SN 2002cx are spectroscopically peculiar because Fe III produces the strongest features (Filippenko et al. 1992b; Ruiz–Lapuente et al. 1992; Jeffery et al. 1992; Mazzali, Danziger, & Turatto 1995; Fisher et al. 1999).

In Figure 12 the spectrum of SN 1999ee is compared with that of the core–normal SN 2001el. SN 1999ee has weaker Si II and S II features, but its HV Ca II is almost as strong as that of SN 2001el (Mazzali et al. 2005a), and the features attributed to HV Fe II are about as strong as in SN 2001el. This is additional support for the HV Fe II identification.

The fitting parameters for the shallow–silicon SNe Ia are in Table 5. The value of $v_e$ is 1000 km s$^{-1}$ except where indicated otherwise in the Table. In Figure 13 the spectrum of SN 1999ee is compared to a synthetic spectrum. The ions used are the same as in the core normals, but with high values of $v_e$ = 4000 km s$^{-1}$ for HV Fe II and 6000 km s$^{-1}$ for O I and HV Ca II.

Figure 11 shows that the spectra of SN 1999ee, SN 1999aw, and SN 2000cx have many similarities at wavelengths longer than about 4300 Å. However, compared to SN 1999ee and SN 1999aw, SN 2000cx is strongly depressed from about 3800 Å to 4200 Å. In Figure 14 the spectrum of SN 2000cx is compared to a synthetic spectrum in which Si II is mildly detached at 15,000 km s$^{-1}$. As in Branch et al. (2004a), HV Ti II is used to provide blocking in the

blue, and to account for the sharp flux peak near 4150 Å. Branch et al. were unable to suggest an identification for the distinct absorption feature near 4530 Å, except for HV H$\beta$, which would be surprising. However, as shown in Figure 15, we now realize that HV Cr II can account for this feature. If the HV Ti II identification is correct, then HV Cr II, at practically the same detachment velocity, is a more plausible identification than H$\beta$. In the synthetic spectrum of Figure 14 HV V II also is introduced, but its main effect is in a crowded spectral region and the identification is not definite.

SN 1991T may be a continuation of the sequence shown in Figure 11; e.g., it bears some resemblance to SN 1999aw, although its Ca II and Si II features are weaker. As further discussed in §7, even though SN 1991T and SN 2002cx are mutual nearest neighbors spectroscopically, in several respects they are quite different. It may be that the only thing these two have in common is a high temperature.

## 7. DISCUSSION

The high degree of spectral homogeneity among the core–normals suggests that they result from a standard, repeatable SN Ia explosion mechanism that does not produce spatially large composition inhomogeneities near the characteristic photospheric velocity of 12,000 km s$^{-1}$ (Thomas et al. 2004). The strong HV Ca II of SN 2001el may involve a spatially large structure near 20,000 km s$^{-1}$ (Kasen et al. 2003; Kasen & Plewa 2005). On the other hand, the features attributed to HV Fe II are only mildly enhanced in SN 2001el and rather homogeneous in the others, suggesting that weak HV Fe II is "natural" in SNe Ia, in the sense that it does not require unusual high–velocity structures (Höflich, Wheeler, & Thielemann 1998, Lentz et al. 2001b). Weak HV Ca II also is ubiquitous (Mazzali et al. 2005b).

Based on previous work (Branch 1987; Benetti et al. 2004) we expected to fit the broad–line SNe Ia with high values of $v_{\rm phot}$, but better fits were obtained by holding $v_{\rm phot}$ constant at 12,000 km s$^{-1}$, a typical value for the core–normals, and using increased $v_{\rm e}$ values. This may be a consequence of nuclear burning extending to higher velocity in the broads than in the core–normals (Lentz et al. 2001a; Benetti et al. 2004; Stehle et al. 2005).

Although the composition structures of the cools surely differ from those of the core–normals (e.g., the low luminosity requires a low mass of $^{56}$Ni), the immediate reason for the spectroscopic differences appears to be the lower temperature. The blue trough in cools, usually referred to as the Ti II trough, is produced not only by Ti II, but also by other ions that appear at low temperature. Ti II is not significant for the 5750 Å absorption.

The 5750 Å absorption of the cools can be accounted for in terms of a high Si II optical depth together with a maximum Si II velocity. This is a plausible way to simultaneously fit these two absorptions while explaining why $R$(Si II) and the ratio of $W(5750)$ to $W(6100)$ go the wrong way with temperature (i.e., increasing with falling temperature), considering that the lower level of $\lambda$5972 is the upper level of $\lambda$6355. If correct, this maximum velocity would indicate that in the cools nuclear burning extends only to unusually low velocities, near 15,000 km s$^{-1}$.

In most of the shallow–silicon SNe Ia the spectral features appear to be produced by the same ions as in the core–normals, although the optical depths are quite different, especially in SN 1991T and SN 2002cx. Most of the differences from core–normals may be caused by a higher temperature. Like SN 2001el among the core–normals, SN 1999ee provides support for the HV Fe II identification. The cause of the depression of the spectra of SN 2000cx in the blue from about 3800 Å to 4200 Å appears to be extra HV line blocking. If HV Ti II is present, then HV Cr II is a more plausible identification than HV H$\beta$ (Branch et al. 2004a) for the 4530 Å absorption in SN 2000cx. As noted in §3, a less distinct absorption appears near 4550 Å even in the core–normals; HV Cr II is a possibility.

One of the most interesting issues that can be addressed by studies of this kind is whether SNe Ia have a continuous distribution of properties, or consist of discrete subgroups. On the whole, we have a sense of continuity. SN 1992A and SN 1981B may be small steps from the core in the direction of SN 1984A; SN 1989B may be a step in the direction of SN 1986G and SN 1991bg; SN 1999ee may be a step in the direction of SN 1991T. If the distribution is continuous, then exactly how the boundaries of the core–normal group are defined is not important.

The cools stand apart from the others in Figure 1, but this in itself does not establish that they differ in kind from the others. As noted by Hatano et al. (2002) and Höflich et al. (2002), there is a temperature threshold below which, owing to abrupt changes in key ionization ratios, line optical depths change abruptly (Hatano et al. 1999). Therefore, the temperature interval required to go from SN 1989B through SN 1986G to SN 1991bg–like events may be narrow. SN 1991bg–like events also are quite subluminous, but especially in the $B$ band, which is strongly blocked by the blue trough. Similarly, there is a temperature threshold above which Fe III features become conspicuous (Hatano et al. 2002). Most SNe Ia may be variations on the basic core–normal theme, with the diversity reflecting differences of degree, rather than differences of kind.

Evidence recently has been presented that in terms of stellar population age there are two SN Ia groups of roughly equal size, one from a young ($\sim 10^8$ years) population and another from another from an older ($\sim$ 3 Gyr) population (Mannucci et al. 2005a; Scannapieco

& Bildsten 2005; Mannucci, Della Valle, & Panagia 2005b). However, we see no basis for splitting the SNe Ia of our sample into two groups of roughly equal size. It may be that there are two different binary–star evolution paths to SNe Ia, one requiring a short time and the other a long time, but with the two paths producing similar outcomes, i.e., carbon–oxygen white dwarfs that explode as they approach the Chandrasekhar mass.

The one event of our sample that does seem to be different in kind is SN 2002cx, which we have placed in the shallow–silicon group. Like SN 1991T it had conspicuous Fe III lines, but unlike SN 1991T it did not have a slow light–curve decline rate and it was subluminous (Li et al. 2003). Its late–time spectra were unlike those of normal SNe Ia, being dominated by very low velocity ($\sim$700 km s$^{-1}$) permitted lines of Fe II, Ca II, Na I, and perhaps O I. Several other SN 2002cx–like events have been discovered (S. Jha et al., in preparation). On the basis of the first–season observations by Li et al. (2003), Branch et al. (2004b) suggested that SN 2002cx may have been a pure deflagration while most other SNe Ia, even SN 1991bg–likes (Höflich et al. 2002), may be delayed detonations or gravitationally confined detonations (Plewa, Calder, & Lamb 2004; Kasen & Plewa 2005). However, the late–time spectra of SN 2002cx (S. Jha et al., in preparation) do not resemble the spectra calculated by Kozma et al. (2005) for one particular 3–D deflagration model, so the nature of SN 2002cx remains uncertain.

The normality of PV features in events such as the core–normal SN 2001el and the shallow–silicon SN 2000cx, both of which have strong HV features, suggests that HV and PV are somewhat independent (with HV Fe II and weak HV Ca II being ubiquitous and natural, as discussed above). An interesting issue for further study is how much of the photometric diversity of SNe Ia is caused by HV features (which may not correlate with luminosity). Another issue is whether the strong HV blue line blocking of SN 2000cx occurs only in the shallow–silicon group. It is clear that strong HV Ca II IR3 absorption occurs not only in the core–normal SN 2001el but also in the shallows.

Our study is complementary to that of Benetti et al. (2005; hereafter Be05), who did not consider the strenths of spectral features. Sixteen events of our sample were included in the study of Be05, who assigned SNe Ia to three groups on the basis of absolute magnitude ($M_B$); light–curve decline rate ($\Delta m_{15}$; Phillips 1993); the blueshift of the 6100 Å absorption 10 days after maximum [$V_{10}$(Si II); Branch & van den Bergh 1993]; the rate at which the 6100 Å absorption drifts to the red [$\dot{v}$(Si II); Be05]; and $R$(Si II). With a few borderline exceptions (SN 1989B and SN 1992A), our cools corresponds to the Be05 FAINT group, which is to be expected since both temperature and luminosity are controlled mainly by the $^{56}$Ni mass. Our broad–line group corresponds to the Be05 HVG (high temporal–velocity gradient) group. This also makes sense because broad 6100 Å absorption requires high Si II

optical depth over a substantial velocity range, which makes it possible for the absorption minimum to shift appreciably with time. The broads appear to have thicker silicon layers than the core–normals. Our core normals and shallows correspond to the Be05 LVG (low temporal–velocity gradient) group. The lower velocity range over which Si II has a high optical depth permits only a smaller shift in the absorption minimum with time.

Polarization observations (Wang et al. 2001; Howell et al. 2001; Wang et al. 2003; Leonard et al. 2005) show that some spectral features are affected by asymmetric structures. A straightforward way to rule out asymmetry as the sole cause of the differences between groups of SNe Ia would be to demonstrate a correlation with parent galaxy type (Be05) or other indicators of the parent–galaxy population (Gallagher et al. 2005). If asymmetry were the sole cause of SN Ia differences, SN Ia subtypes would not correlate with galaxy types. But, in fact, there are correlations and emerging correlations. SN 1991bg–like events tend to occur in older populations (Howell 2001). In the Be05 sample the mean host galaxy morphological type (the T type) was found to increase from the FAINT to HVG to LVG groups. Similarly, for our sample the mean T type increases from cools to core–normals to broads to shallows, but the statistics are too poor to allow definite conclusions.

The expected rapid increase in the number of well observed SNe Ia in the near future (e.g., Wood–Vasey et al. 2004) will allow the relationships among SNe Ia to be clarified. We expect that our Paper III (in preparation), on premaximum spectra, also will clarify the view presented here.

We are grateful to all observers who have provided spectra. This work has been supported by NSF grants AST-0204771 and AST-0506028, and NASA LTSA grant NNG04GD36G.

## A. Measuring Spectral Difference

In order to quantify difference in spectral features we use the scaled–tilted spectrum expressed by flux values $\tilde{y}_{\ell i}$ for wavelengths $\lambda_i$ which are parameterized as

$$\tilde{y}_{\ell i} = S_\ell y_{\ell i} \left( \frac{\lambda_i}{\lambda_0} \right)^{\alpha_\ell} . \tag{A1}$$

The $y_{\ell i}$ values are the observed spectral flux values of spectrum $\ell$. The factor $S_\ell$ is a scale factor and the factor $(\lambda_i/\lambda_0)^{\alpha_\ell}$ produces tilt; $\lambda_0$ is just a reference wavelength that need not actually be specified. (This scaling and tilting of spectra is more elaborate than the tilting we describe in the main text (see § 1) for spectra that we present and fit with **Synow** spectra.)

For two spectra labeled by indexes 1 and 2, we formulate the $\chi^2$–like function:

$$\begin{aligned}
\chi^2 &= \sum_i \left\{ \log\left[ S_2 y_{2i} \left( \frac{\lambda_i}{\lambda_0} \right)^{\alpha_2} \right] - \log\left[ S_1 y_{1i} \left( \frac{\lambda_i}{\lambda_0} \right)^{\alpha_1} \right] \right\}^2 \\
&= \sum_i \left\{ \log\left[ \left( \frac{S_2}{S_1} \right) \left( \frac{y_{2i}}{y_{1i}} \right) \left( \frac{\lambda_i}{\lambda_0} \right)^{\alpha_2 - \alpha_1} \right] \right\}^2 \\
&= \sum_i \left( s + f_i + \alpha w_i \right)^2 \\
&= \sum_i \left( s^2 + f_i^2 + \alpha^2 w_i^2 + 2 s f_i + 2 s \alpha w_i + 2 \alpha f_i w_i \right) \\
&= s^2 N + F_f + \alpha^2 W_w + 2 s F + 2 s \alpha W + 2 \alpha F_w \ , \qquad \text{(A2)}
\end{aligned}$$

where

$$s = \log\left( \frac{S_2}{S_1} \right) \ , , \qquad f_i = \log\left( \frac{y_{2i}}{y_{1i}} \right) \ , \qquad w_i = \log\left( \frac{\lambda_i}{\lambda_0} \right) \ , \qquad \alpha = \alpha_2 - \alpha_1 \ , \qquad \text{(A3)}$$

$$N = \text{number of spectral points} \ , \qquad \text{(A4)}$$

$$F_f = \sum_i f_i^2 \ , \qquad W_w = \sum_i w_i^2 \ , \qquad F = \sum_i f_i \ , \qquad W = \sum_i w_i \ , \qquad \text{(A5)}$$

and

$$F_w = \sum_i f_i w_i \ . \qquad \text{(A6)}$$

To minimize the $\chi^2$, we find the partial derivatives.

$$\frac{\partial \chi^2}{\partial s} = 2(sN + F + \alpha W) \qquad \text{and} \qquad \frac{\partial \chi^2}{\partial \alpha} = 2(\alpha W_w + sW + F_w) \ . \qquad \text{(A7)}$$

Setting these equations equal to zero and solving we find the $s$ and $\alpha$ values that give the stationary point of $\chi^2$:

$$s = \frac{W_w F - W F_w}{W^2 - W_w N} \qquad \text{and} \qquad \alpha = \frac{WF - N F_w}{N W_w - W^2} \ . \qquad \text{(A8)}$$

Since the stationary point is unique and $\chi^2$ must have an analytic global minimum with respect to $s$ and $\alpha$, equation (A8) gives the global minimizing values of $s$ and $\alpha$.

## REFERENCES

Barbon, R., Iijima, T., & Rosino, L. 1989, A&A, 220, 83

Baron, E., Lentz, E. J., & Hauschildt, P. H. 2003, ApJ, 588, L29

Benetti, S., et al. 2004, MNRAS, 348, 261

Benetti, S., et al. 2005, ApJ, 623, 1011

Branch, D. 1987, ApJ, 316, L81

Branch, D., Baron, E., Hall, N., Melakayil, M., & Parrent, J. 2005, PASP, 117, 545; Paper I

Branch, D., Lacy, M. L., McCall, M. L., Sutherland, P. G., Uomoto, A., Wheeler, J. C., & Wills, B. J. 1983, ApJ, 270, 123

Branch, D., & van den Bergh, S. 1993, AJ, 105, 2231

Branch, D., et al. 2003, AJ, 126, 1489

Branch, D., et al. 2004a, ApJ, 606, 413

Branch, D., et al. 2004b, PASP, 116, 903

Cristiani, S. et al. 1992, A&A, 259, 63

Filippenko, A. V., et al. 1992a, AJ, 104, 1543

Filippenko, A. V., et al. 1992b, ApJ, 384, L15

Fisher, A., Branch, D., Katano, K., & Baron, E. 1999, MNRAS, 304, 67

Gallagher, J. S., Garnavich, P. M., Berlind, P., Challis, P., Jha, S., & Kirshner, R. P. 2005, ApJ, in press

Garnavich, P. M., et al. 2004, ApJ, 613, 1120

Gomez, G., Lopez, R., & Sanchez, F. 1996, AJ, 112, 2094

Hamuy, M., et al. 2002, AJ, 124, 417

Hatano, K., Branch, D., Fisher, A., Millard, J., & Baron, E. 1999, ApJS, 121, 233

Hatano, K., Branch, D., Qiu, Y. L., Baron, E., Thielemann, F.-K., & Fisher, A. 2002, New Astr., 7, 441

Hernandez, M., et al. 2000, MNRAS, 319, 223

Höflich, P., Gerardy, C. L., Fesen, R. A., & Sakai, S. 2002, ApJ, 568, 791

Höflich, P., Wheeler, J. C., & Thielemann, F.-K. 1998, ApJ, 495, 617

Howell, D. A. 2001, ApJ, 554, L193

Howell, D. A., Höflich, P., Wang, L., & Wheeler, J. C. 2001, ApJ, 556, 302

Howell, D. A., & Nugent, P. 2004, in Cosmic Explosions in Three Dimensions, eds. P. Höflich, P. Kumar, & J. C. Wheeler (Cambridge, CUP), p. 151

Jeffery, D. J., Leibundgut, B., Kirshner, R. P., Benetti, S., Branch, D., & Sonneborn, G. 1992, ApJ, 397, 304

Kasen, D., & Plewa, T. 2005, ApJ, 622, L41

Kasen, D., et al. 2003, ApJ, 593, 788

Kozma, C., et al. 2005, A&A, 437, 983

Kurucz, R. L. 1993, CD-ROM 1, Atomic Data for Opacity Calculations (Cambridge: SAO)

Lentz, E. J., Baron, E., Branch, D., & Hauschildt, P. H. 2001a, ApJ, 547, 402

Lentz, E. J., Baron, E., Branch, D., & Hauschildt, P. H. 2001b, ApJ, 557, 266

Leonard, D. C., Li, W., Filippenko, A. V., Foley, R. J., & Chornock, R. 2005, ApJ, 632, 450

Li, W., et al. 2002, PASP, 113, 1178

Li, W., et al. 2003, PASP, 115, 453

Mannucci, F., Della Valle, M., & Panagia, N. 2005b, MNRAS, in press

Mannucci, F., et al. 2005a, A&A, 433, 807

Mazzali, P. A., Danziger, I. J., & Turatto, M. 1995, A&A 297, 509

Mazzali, P. A., et al. 1997, MNRAS, 284, 151

Mazzali, P. A., et al. 2005a, MNRAS, 357, 200

Mazzali, P. A., et al. 2005b, ApJ, 623, L37

Meikle, W. P. S., et al. 1996, MNRAS, 281, 263

Nugent, P., Phillips, M. M., Baron, E., Branch, D., & Hauschildt, P. H. 1995, ApJ, 455, L147

Phillips, M. M. 1979, ApJS, 39, 377

Phillips, M. M. 1992, AJ, 103, 1632

Phillips, M. M. 1993, ApJ, 413, L105

Plewa, T., Calder, A. C., & Lamb, D. Q. 2004, ApJ, 612, L37

Ruiz–Lapuente et al. 1992, ApJ, 387, L33

Salvo, M. E., Cappellaro, E., Mazzali, P. A., Benetti, S., Danziger, I. J., Pata, F., & Turatto, M. 2001, MNRAS, 321, 254

Scannapieco, E., & Bildsten, L. 2005, ApJ, 629, L85

Thomas, R. C., Branch, D., Baron, E., Nomoto, K., Li, W., & Filippenko, A. V. 2004, ApJ, 601, 1019

Turatto, M., Piemonte, A., Benetti, S., Cappellaro, E., Mazzali, P. A., Danziger, I. J., & Patat, F. 1998, ApJ, 116, 2431

Vacca, W. D., & Leibundgut, B. 1996, ApJ, 471, L37

Wang, L., Howell, D. A., Höflich, P, & Wheeler, J. C. 2001, ApJ, 550, 1030

Wang, L., et al. 2003, ApJ, 591, 1110

Wells, L. A., et al. 1994, AJ, 108, 2233

Wood–Vasey, W. M., et al. 2004, New Astr. Rev., 48, 637

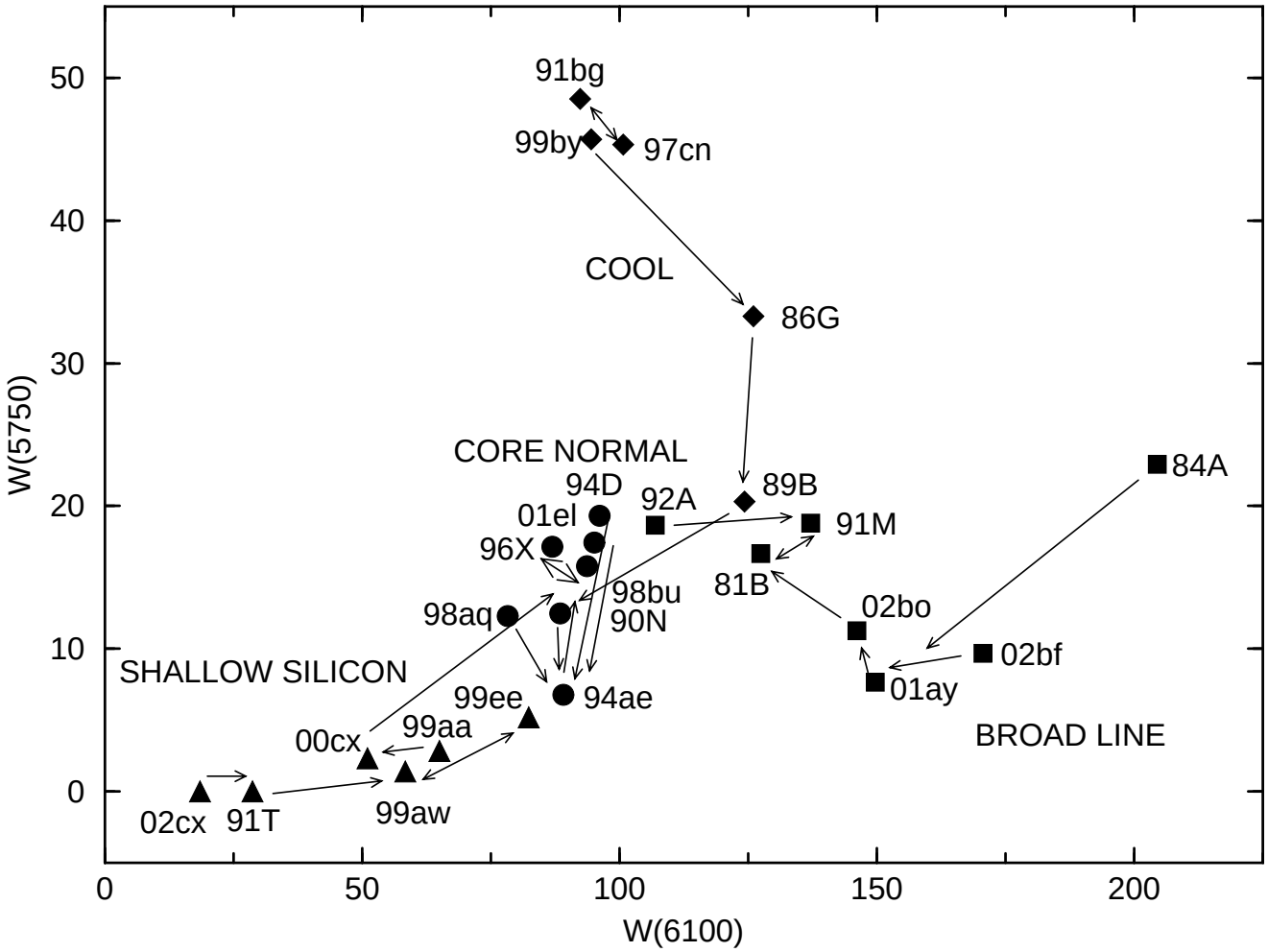


Fig. 1.— $W(5750)$ is plotted against $W(6100)$. *Single–headed arrows* point to nearest neighbors (see text). *Double–headed arrows* connect mutual nearest neighbors. Core–normal SNe Ia are shown as *circles*, broad–line SNe Ia as *squares*, cool SNe Ia as *diamonds*, and shallow–silicon SNe Ia as *triangles*.

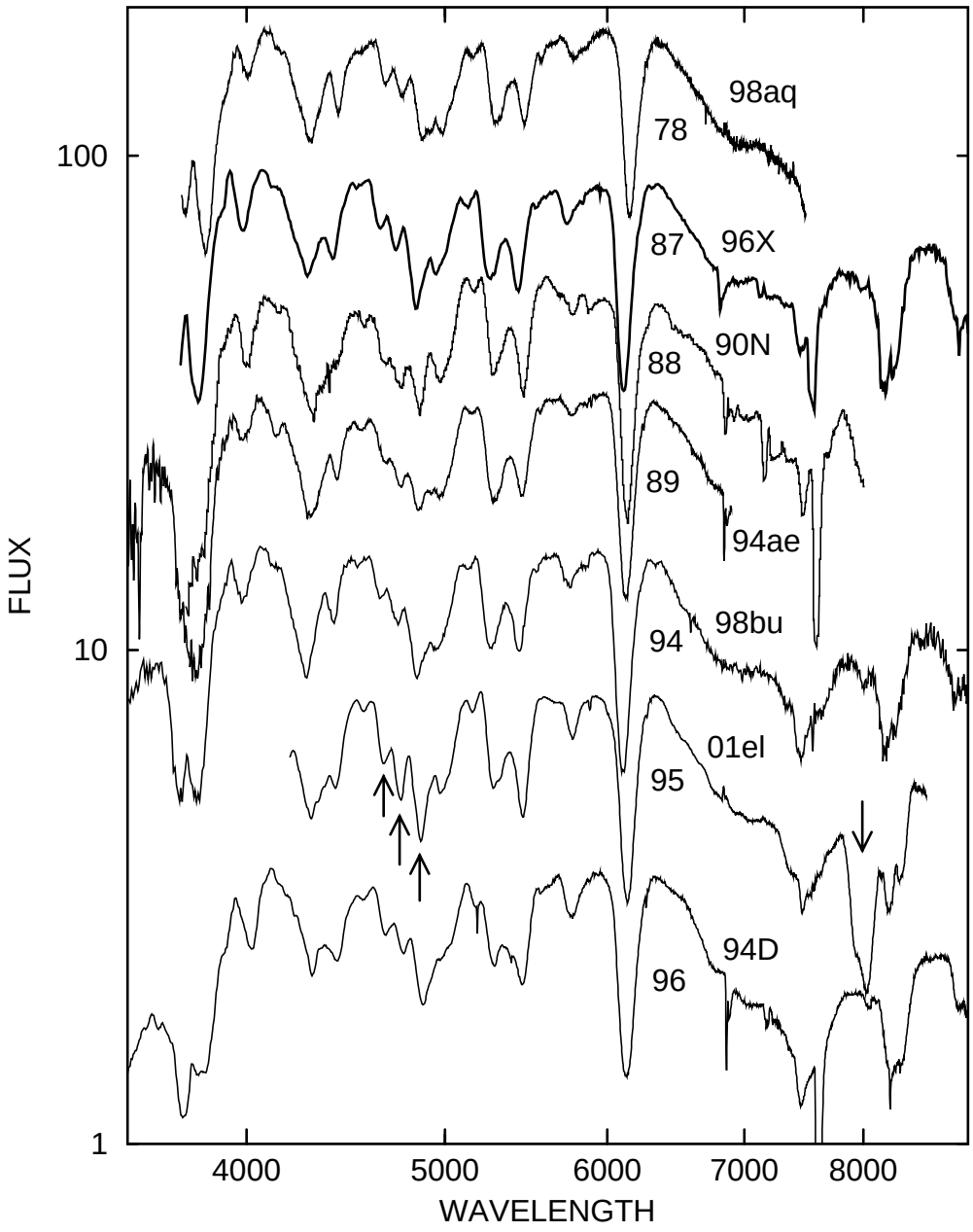


Fig. 2.— Spectra of seven core–normals, ordered according to increasing $W(6100)$ from top to bottom; the $W(6100)$ values are shown adjacent to the 6100 Å absorptions. The spectra have been tilted to make the flux peaks near 4600 Å and 6300 Å equally high. Vertical displacements are arbitrary. Narrow absorptions near 7600 Å and 6900 Å are telluric. The only conspicuous difference among these spectra is the strong high–velocity Ca II IR3 absorption near 8000 Å in SN 2001el (*downward arrow*). Three less conspicuous differences (*upward arrows*), also in SN 2001el, are attributed (see text) to high–velocity Fe II.

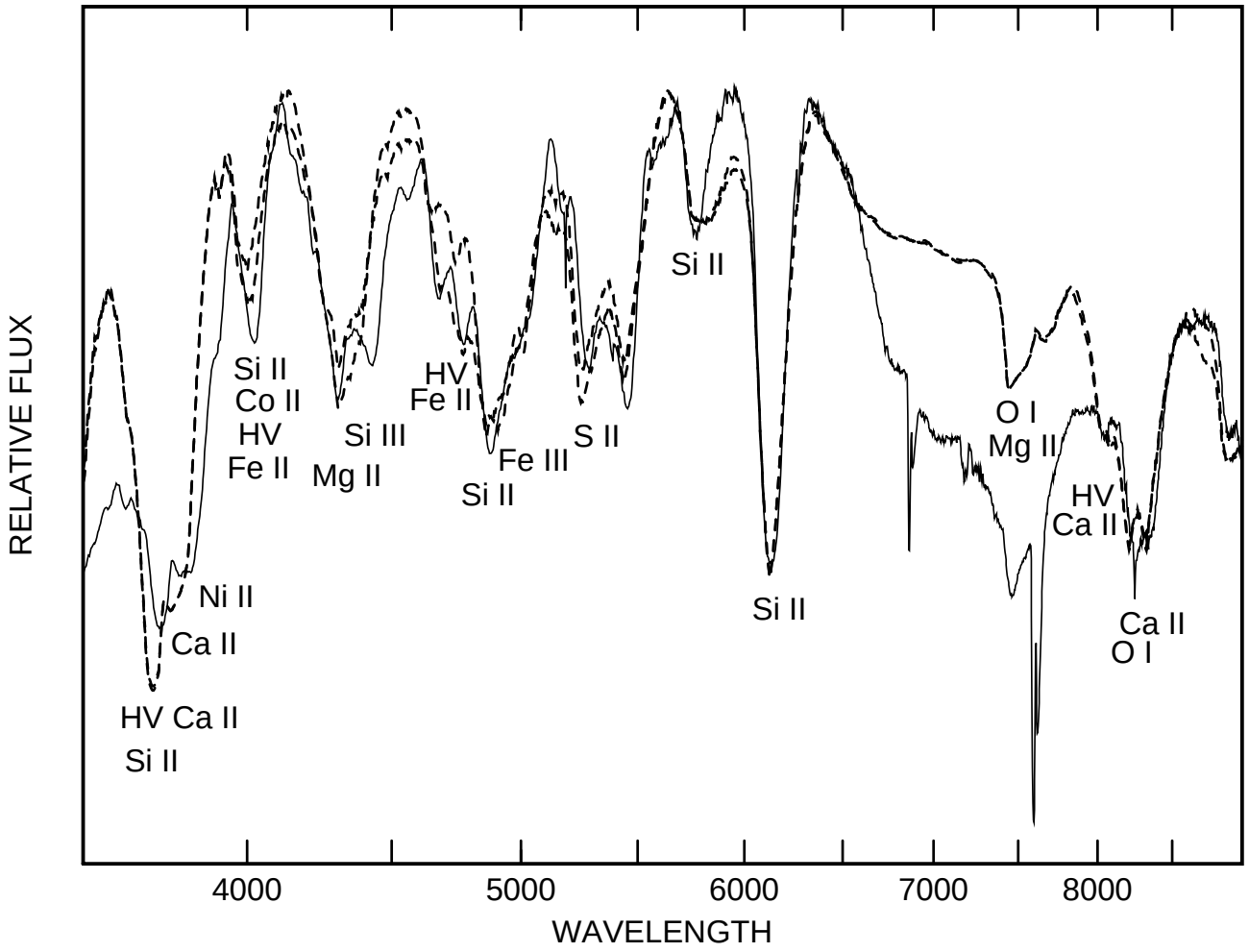


Fig. 3.— The spectrum of SN 1994D (*solid line*) is compared with two synthetic spectra (*dashed lines*). One includes HV Fe II and the other does not. The main difference in the synthetic spectra is due to HV Fe II absorption between 4600 Å and 4800 Å.

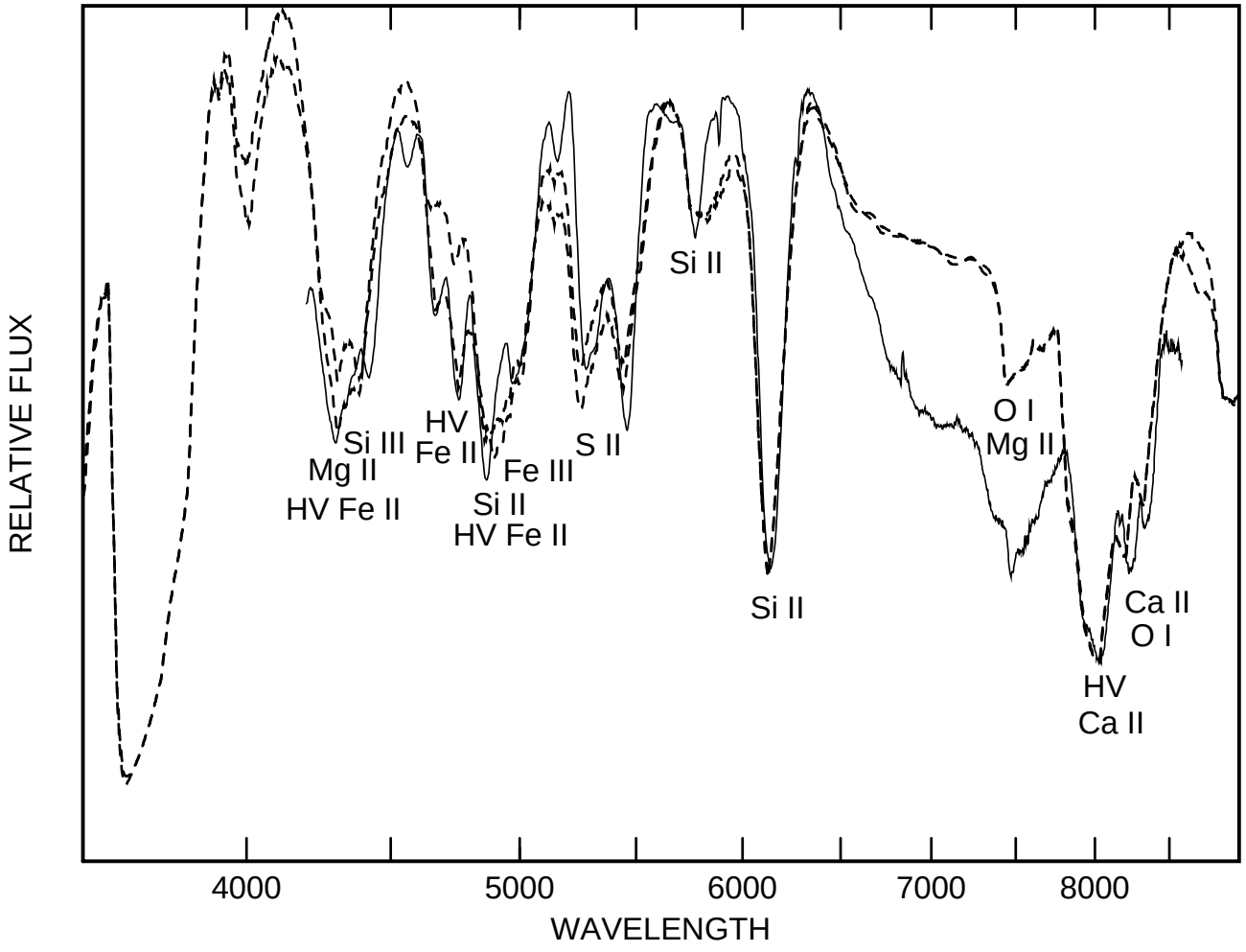


Fig. 4.— The spectrum of SN 2001el (*solid line*) is compared with synthetic spectra (*dashed lines*) that do and do not include HV Fe II.

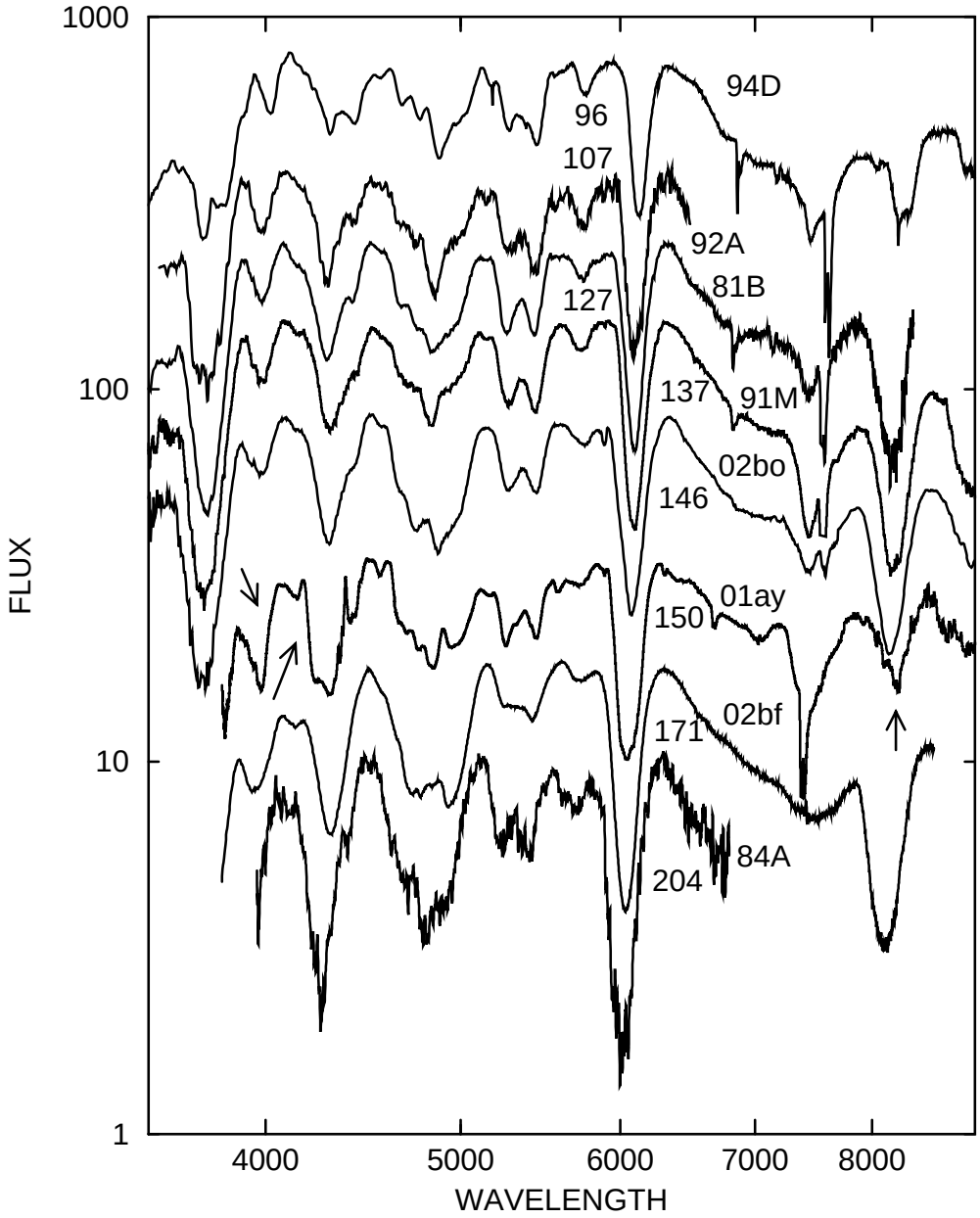


Fig. 5.— Spectra of the core–normal SN 1994D and seven broad–line SNe Ia. Three *arrows* indicate some of the differences between SN 2001ay and the others.

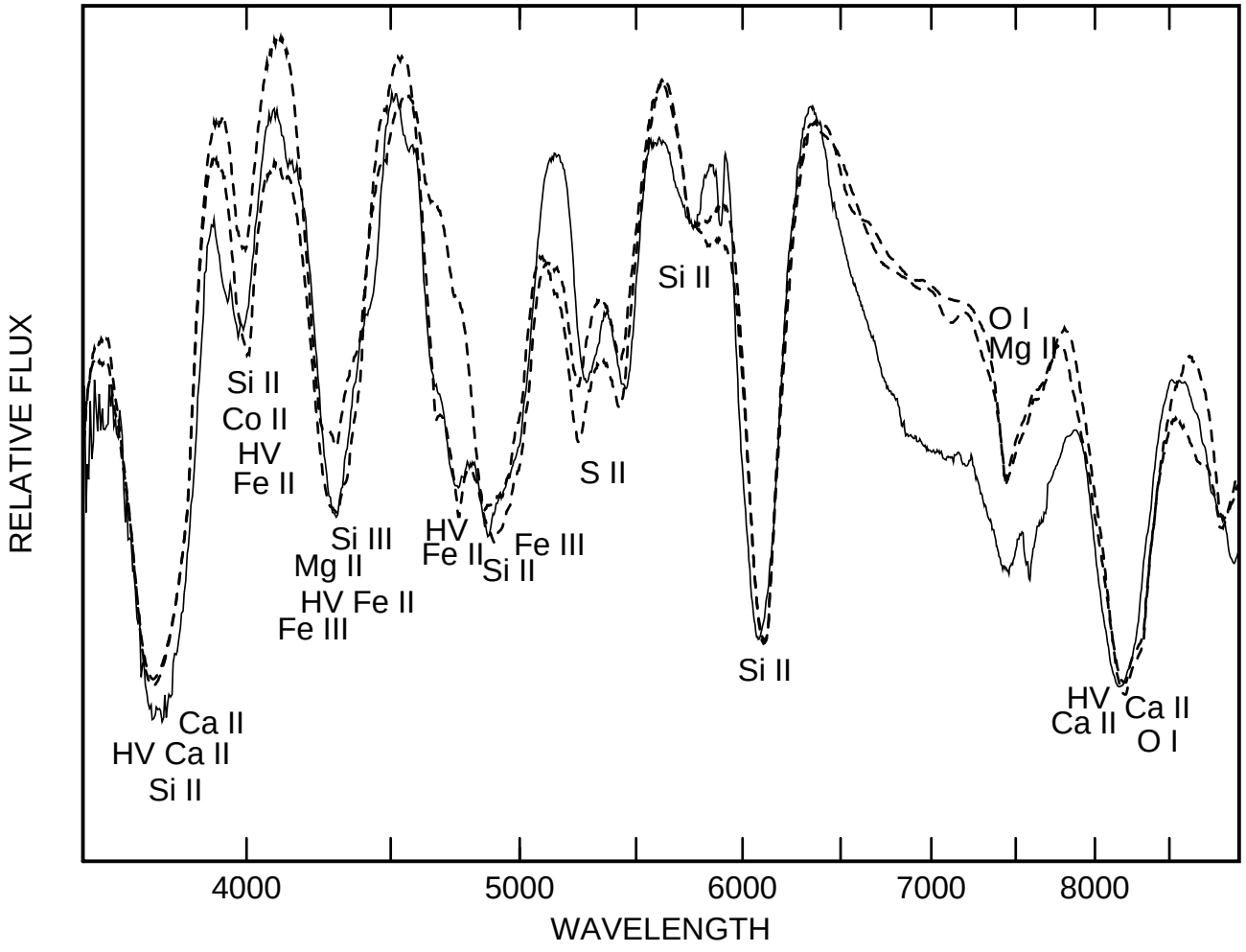


Fig. 6.— The spectrum of SN 2002bo (*solid line*) is compared with synthetic spectra (*dashed lines*) that do and do not include HV Fe II.

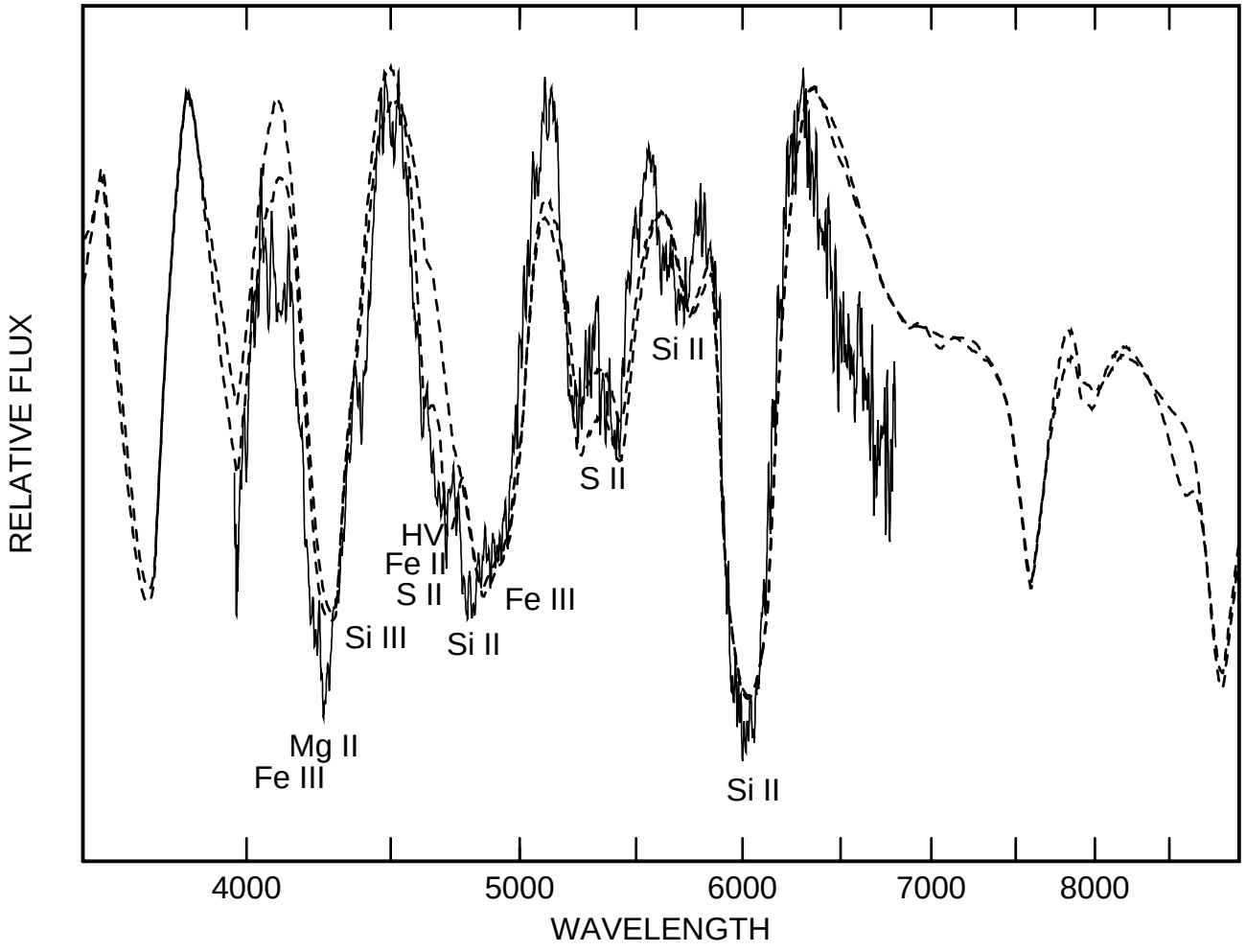


Fig. 7.— The spectrum of SN 1984A (*solid line*) is compared with synthetic spectra (*dashed lines*) that do and do not include HV Fe II.

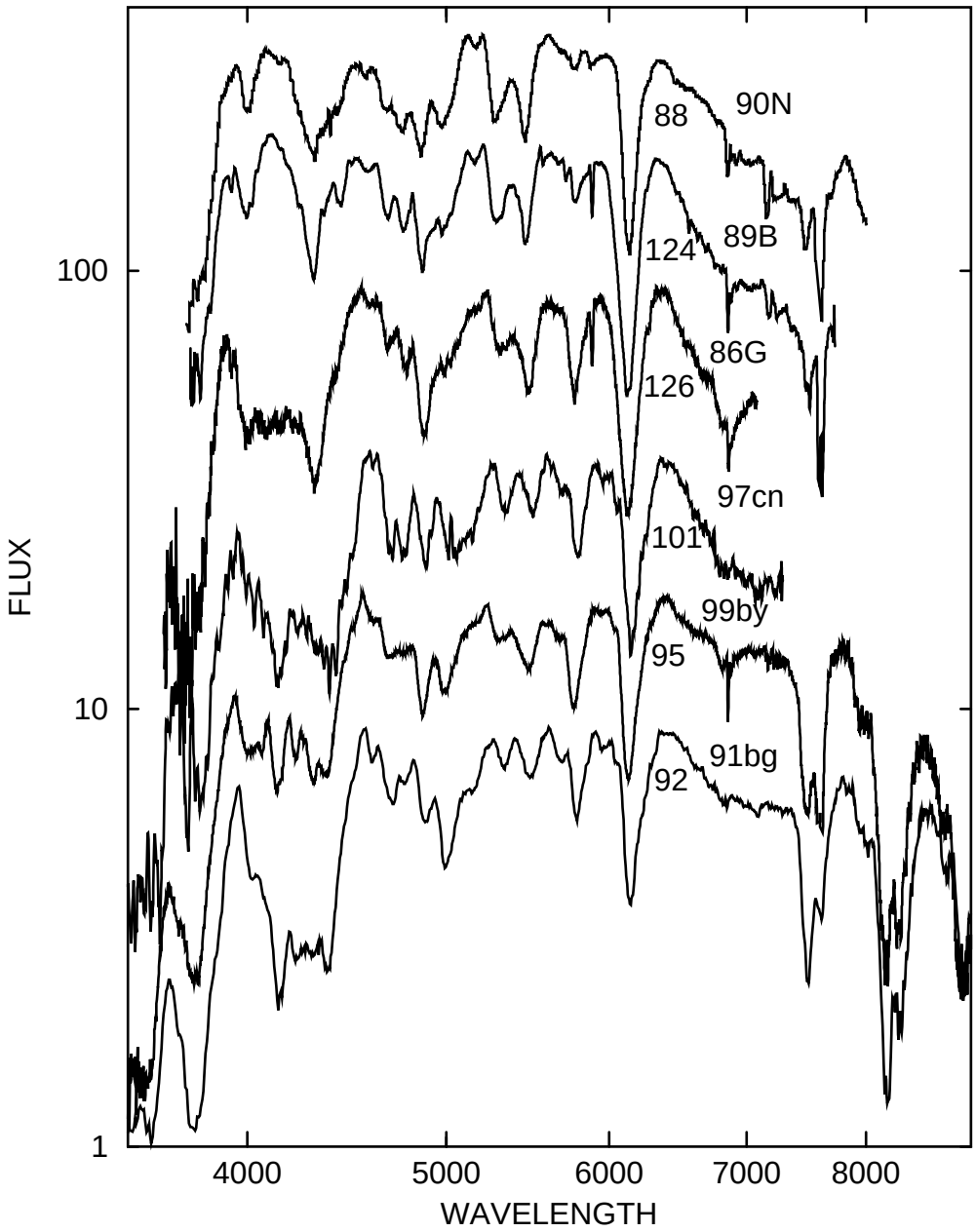


Fig. 8.— Spectra of the core–normal SN 1990N and five cool SNe Ia.

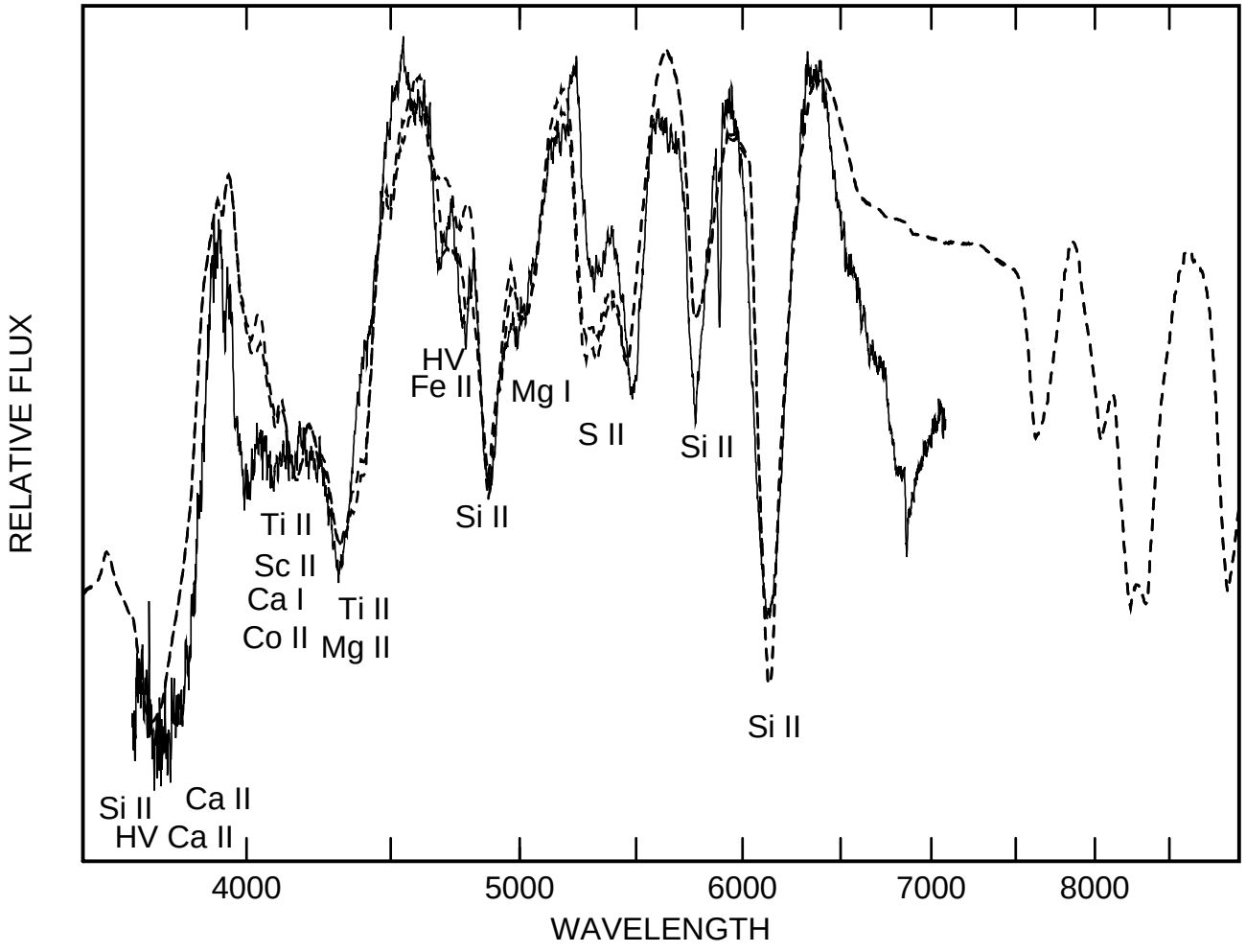


Fig. 9.— The spectrum of SN 1986G (*solid line*) is compared with synthetic spectra (*dashed lines*) that do and do not include HV Fe II.

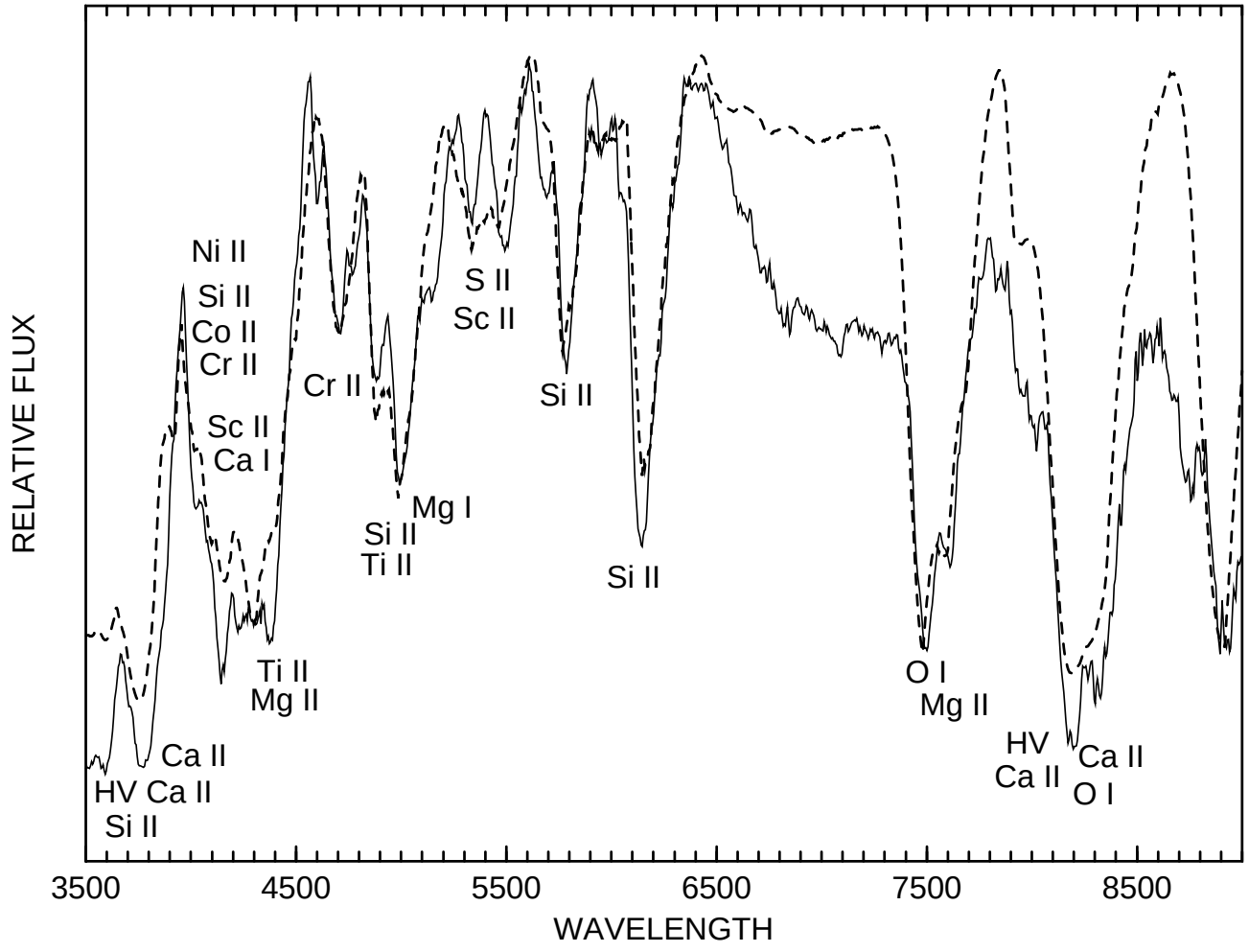


Fig. 10.— The spectrum of SN 1991bg (*solid line*) is compared with a synthetic spectrum (*dashed line*).

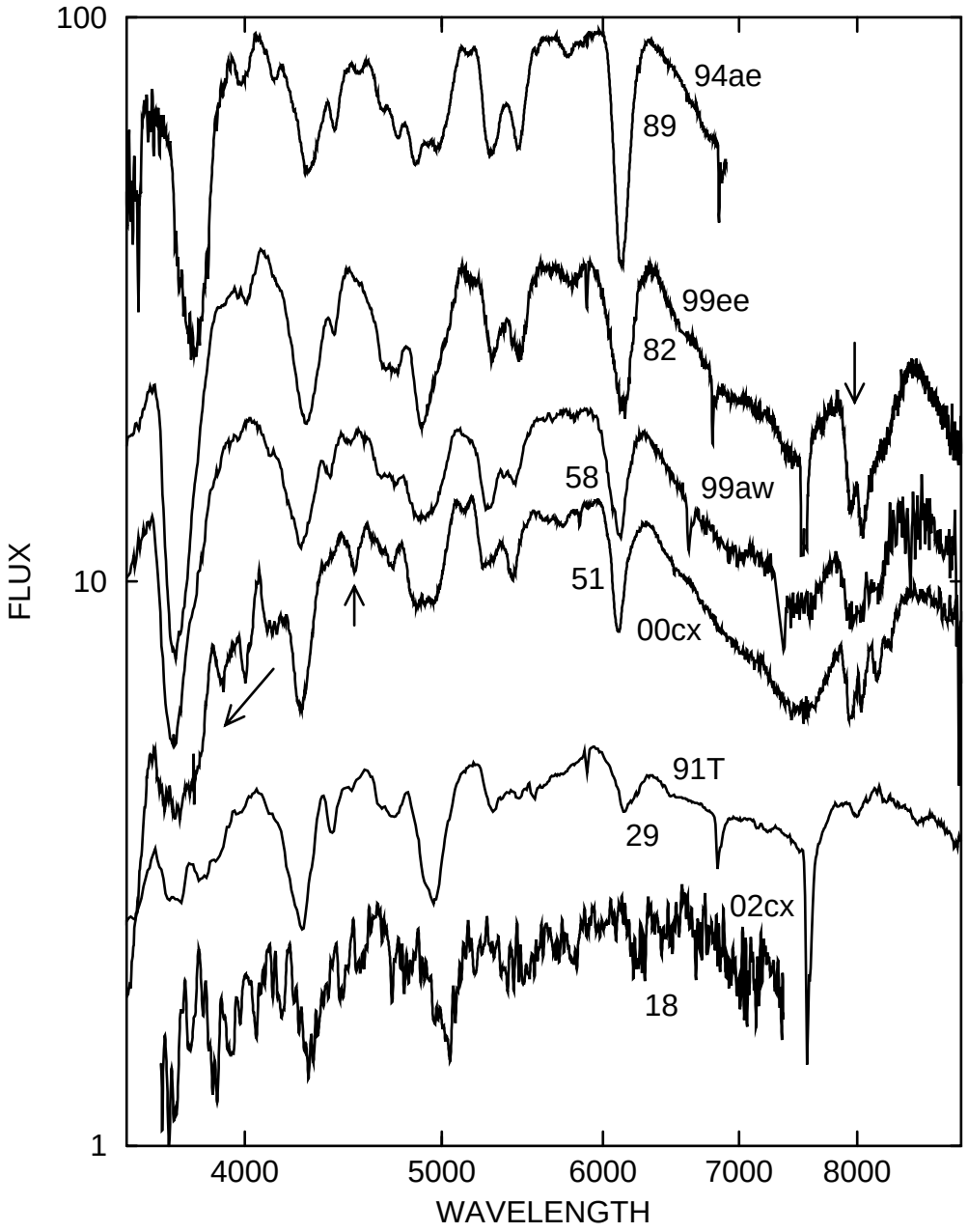


Fig. 11.— Spectra of the core–normal SN 1994ae and five shallow–silicon SNe Ia. *Arrows* indicate (from right to left) the strong HV Ca II IR3 absorption in SN 1999ee; the distinct 4530 Å absorption in SN 2000cx; and the depression of the spectrum of SN 2000cx from about 3800 Å to 4200 Å.

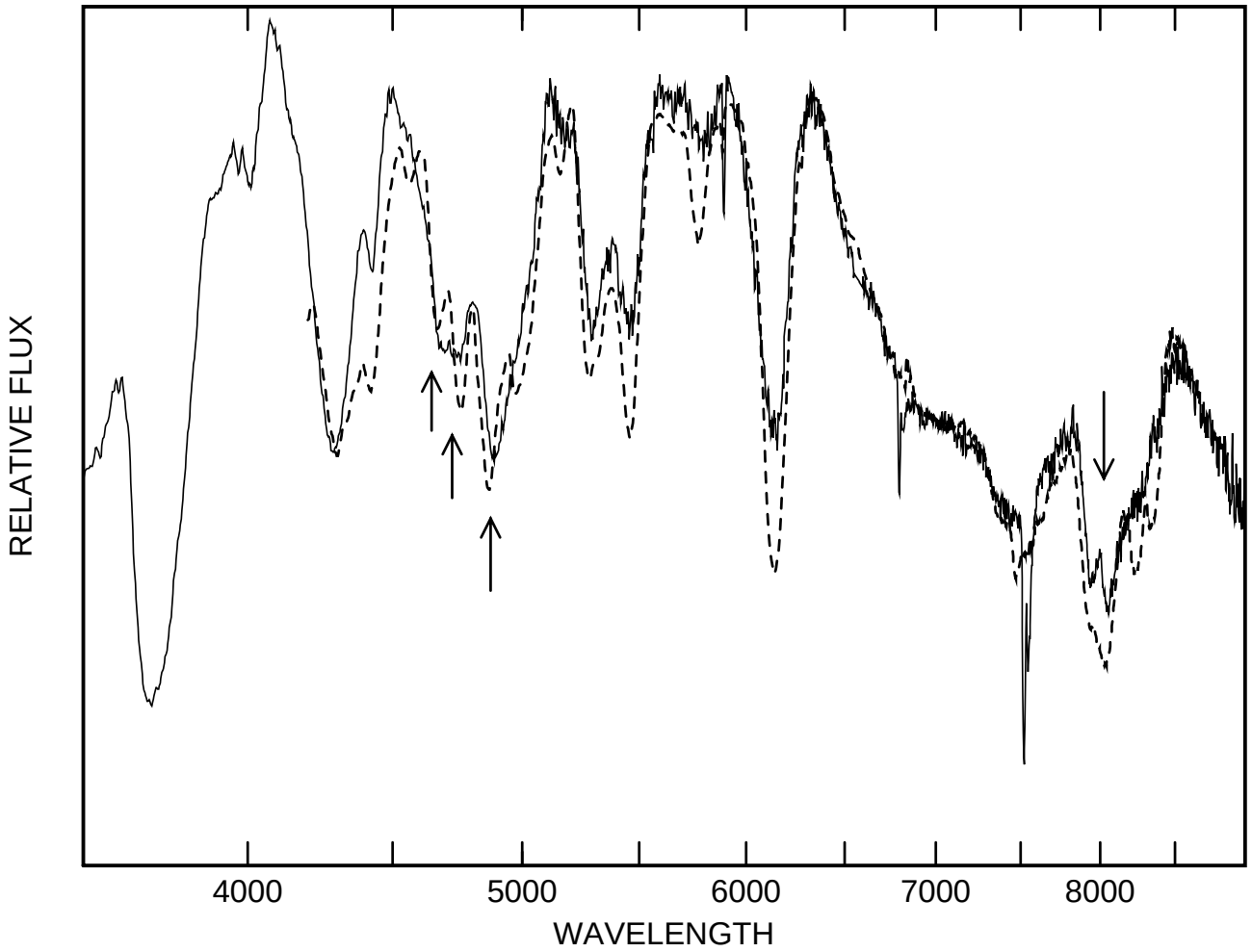


Fig. 12.— The spectra of SN 1999ee (*solid line*) and SN 2001el (*dashed line*) are compared. *Arrows* indicate strong Ca II IR3 absorption and enhanced HV Fe II absorption in both supernovae.

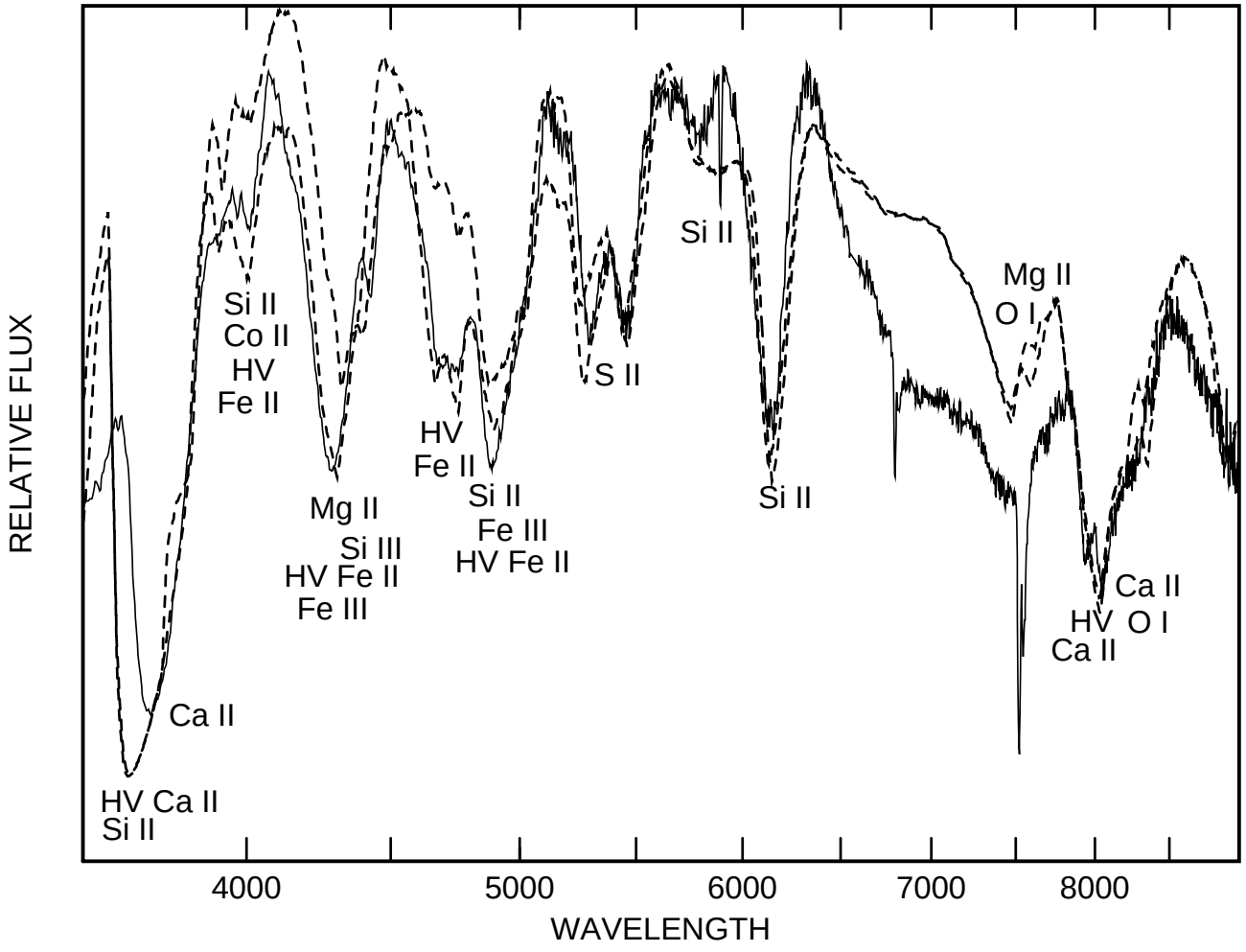


Fig. 13.— The spectrum of SN 1999ee (*solid line*) is compared with synthetic spectra (*dashed lines*) that do and do not include HV Fe II.

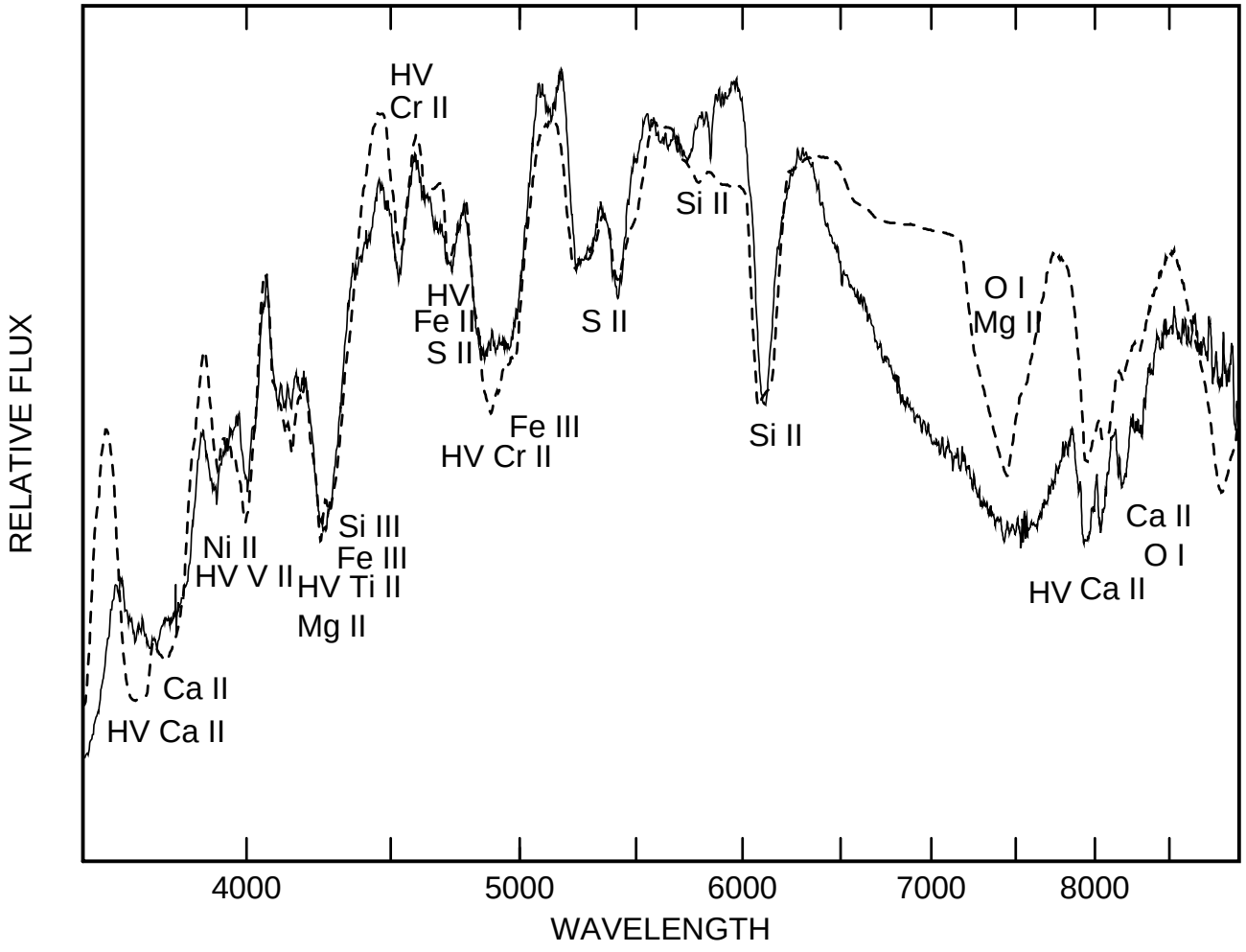


Fig. 14.— The spectrum of SN 2000cx (*solid line*) is compared with a synthetic spectrum (*dashed line*).

Table 1. The SN Ia Sample

| SN | epoch (days) | galaxy | $W(6100)$ ( Å) | $W(5750)$ ( Å) | reference |
|---|---|---|---|---|---|
| 1981B | −2 | NGC 4536 | 127 | 17 | Branch et al. (1983) |
| 1984A | −3 | NGC 4419 | 204 | 23 | Barbon et al. (1989) |
| 1986G | −1 | NGC 5128 | 126 | 33 | Cristiani et al. (1992) |
| 1989B | 0 | NGC 3627 | 124 | 20 | Wells et al. (1994) |
| 1990N | −2 | NGC 4639 | 88 | 12 | Asiago SN Group |
| 1991M | 3 | IC 1151 | 137 | 19 | Gomez et al. (1996) |
| 1991T | −3 | NGC 4527 | 29 | 0 | Phillips et al. (1992) |
| 1991bg | 0 | NGC 4374 | 92 | 49 | Filippenko et al. (1992a) |
| 1992A | −1 | NGC 1380 | 107 | 19 | P. Challis, unpublished |
| 1994D | −1 | NGC 4526 | 96 | 19 | Meikle et al. (1996) |
| 1994ae | 0 | NGC 3370 | 89 | 7 | Howell & Nugent (2004) |
| 1996X | −2 | NGC 5061 | 87 | 17 | Salvo et al. (2001) |
| 1997cn | 3 | NGC 5490 | 101 | 45 | Turatto et al. (1998) |
| 1998aq | 0 | NGC 3982 | 78 | 12 | Branch et al. (2003) |
| 1998bu | −1 | NGC 3368 | 94 | 16 | Hernandez et al. (2000) |
| 1999aw | 3 | − − − | 58 | 1 | Howell & Nugent (2004) |
| 1999by | −3 | NGC 2841 | 95 | 46 | Garnavich et al. (2004) |
| 1999ee | −2 | IC 5179 | 82 | 5 | Hamuy et al. (2002) |
| 2000cx | 2 | NGC 524 | 51 | 2 | Li et al. (2002) |
| 2001ay | 0 | IC 4423 | 150 | 8 | Howell & Nugent (2004) |
| 2001el | 1 | NGC 1448 | 95 | 16 | Wang et al. (2003) |
| 2002bf | 3 | − − − | 171 | 10 | Leonard et al. (2005) |
| 2002bo | −1 | NGC 3190 | 146 | 11 | Benetti et al. (2004) |
| 2002cx | −1 | −−− | 18 | 0 | Li et al. (2003) |

Table 2. Fitting Parameters for Core–Normals

| | SN 1998aq | SN 1996X | SN 1990N | SN 1994ae | SN 1998bu | SN 2001el | SN 1994D |
|---|---|---|---|---|---|---|---|
| $v_{\rm phot}$ (km s$^{-1}$) | 12,000 | 13,000 | 12,000 | 12,000 | 13,000 | 12,000 | 12,000 |
| $v_{\rm e}$ (km s$^{-1}$) | 1000 | 1000 | 1000 | 1000 | 1000 | 1000 | 1000 |
| $T_{\rm exc}$ (K) | 10,000 | 10,000 | 10,000 | 10,000 | 10,000 | 10,000 | 10,000 |
| $\tau$(O I) | | 0.7/14 | 0.5/14 | | 0.7/14 | 0.5/14 | 0.5/14 |
| $\tau$(Mg II) | 1.5 | 1.2 | 1.7 | 1.3 | 2 | 1.5 | 1.2 |
| $\tau$(Si II) | 6 | 13 | 11 | 8 | 13 | 12 | 12 |
| $\tau$(Si III) | 1.7 | 0.8 | 1 | 1.2 | 0.6 | 1.7 | 0.6 |
| $\tau$(S II) | 2 | 2.5 | 2.3 | 2.4 | 2.3 | 2.5 | 2.3 |
| $\tau$(Ca II) | 80 | 80 | 80 | 80 | 80 | 120 | 80 |
| $\tau$(HV Ca II) | | 2(2)/21 | | | 5(2)/21 | 12(12)/19[30] | 3(2)/20 |
| $\tau$(HV Fe II) | 0.5(2)/16 | 0.3(2)/18 | 0.6(2)/17 | 0.5(2)/17 | 0.3(2)/18 | 0.8(2)/17 | 0.7(2)/16 |
| $\tau$(Fe III) | 1.5 | 1.5 | 0.8 | 1.2 | 1.5 | 1.2 | 0.8 |
| $\tau$(Co II) | 0.6 | 0.6 | 0.4 | 0 | 0.6 | | 0.8 |
| $\tau$(Ni II) | 0.7 | 0.2 | 0.8 | 0.5 | 0.5 | | 0.6 |

[a]For each ion the optical depth, $\tau$, is the optical depth at the photosphere or the detachment velocity of the ion's reference line (ordinarily the ion's strongest line in the optical spectrum). When a value of $v_{\rm e}$ other than the default value in row 2 is used, the value (in units of 1000 km s$^{-1}$) is given in parentheses. Minimum and maximum velocities (in units of 1000 km s$^{-1}$) are preceded by a forward slash. Maximum velocities are in square brackets. The absence of an optical–depth entry means that the observed spectrum does not include

the relevant wavelength range.

Table 3. Fitting Parameters for Broad–Line SNe Ia

| | SN 1992A | SN 1981B | SN 1991M | SN 2002bo | SN 2001ay | SN 2002bf | SN 1984A |
|---|---|---|---|---|---|---|---|
| $v_{\rm phot}$ (km s$^{-1}$) | 12,000 | 12,000 | 12,000 | 12,000 | 12,000 | 12,000 | 12,000 |
| $v_{\rm e}$ (km s$^{-1}$) | 2000 | 2000 | 2000 | 2000 | 2000 | 2000 | 2000 |
| $T_{\rm exc}$ (K) | 10,000 | 10,000 | 10,000 | 10,000 | 10,000 | 10,000 | 10,000 |
| $\tau$(O I) | 0.5/14 | 0.5/14 | 0.5/14 | 0.5/14 | 0.5(4) | 0.3(10) | 0 |
| $\tau$(Mg II) | 1.2 | 1 | 1 | 1 | 1(4) | 2(4) | 5 |
| $\tau$(Si II) | 8 | 8 | 8 | 8 | 3(4) | 4(5)/[22] | 6(5)/[25] |
| $\tau$(Si III) | 0.4 | 0.6 | 0.6 | 0.0 | 0.4 | 0.6 | 0.6 |
| $\tau$(S II) | 1.5 | 1.5 | 1.5 | 1.5 | 1 | 0.7 | 1.5 |
| $\tau$(Ca II) | 100 | 60 | 100 | 120 | 12 | 150 | |
| $\tau$(HV Ca II) | 2/21 | 5/21 | 2/21 | 3(3)/21 | 0 | 40(3)/18[30] | |
| $\tau$(HV Fe II) | 0.6/17 | 0.6/17 | 0.6/17 | 1.5(3)/17 | 0.3/17 | 2(3)/17 | 1(3)/20 |
| $\tau$(Fe III) | 0.5 | 1 | 0.2 | 1.2 | 0.3 | 1.2 | 2 |
| $\tau$(Co II) | 1 | 1 | 1 | 1 | 1 | 1 | |
| $\tau$(Ni II) | 0.2 | 0.2 | 0.2 | 0.2 | | 0.2 | |

Table 4. Fitting Parameters for Cool SNe Ia

| | SN 1989B | SN 1986G | SN 1997cn | SN 1999by | SN 1991bg |
|---|---|---|---|---|---|
| $v_{\rm phot}$ (km s$^{-1}$) | 11,000 | 11,000 | 11,000 | 11,000 | 11,000 |
| $v_{\rm e}$ (km s$^{-1}$) | 1000 | 1000 | 1000 | 1000 | 1000 |
| $T_{\rm exc}$ (K) | 10,000 | 7000 | 7000 | 7000 | 7000 |
| $\tau$(O I) | 0.5/12 | | | 12/12 | 18/12 |
| $\tau$(Na I) | 0 | 0 | 0.3/12 | 0.5/12 | 0.3/12 |
| $\tau$(Mg I) | 0 | 3 | 2/12 | 3.5/12 | 7/12 |
| $\tau$(Mg II) | 4 | 8 | 20/12 | 20/12 | 30/12 |
| $\tau$(Si II) | 15 | 100/[15] | 300/[13] | 150/[14] | 200/[13] |
| $\tau$(Si III) | 0.6 | 0 | 0 | 0 | 0 |
| $\tau$(S II) | 2.3 | 2 | 0.8 | 1 | 0.5 |
| $\tau$(Ca I) | 0 | 8 | 10 | 10 | 10 |
| $\tau$(Ca II) | 120 | 500 | 5000 | 5000 | 5000 |
| $\tau$(HV Ca II) | | 10(2)/19 | 50/16 | 50/16 | 50/16 |
| $\tau$(Sc II) | 0 | 8 | 10 | 10 | 10 |
| $\tau$(Ti II) | 0 | 2.5 | 5 | 4 | 4 |
| $\tau$(Cr II) | 0 | 0 | 2 | 2 | 2 |
| $\tau$(HV Fe II) | 0.6(2)/17 | 1/15 | 1/17 | 0 | 0 |
| $\tau$(Fe III) | 1 | 0 | 0 | 0 | 0 |
| $\tau$(Co II) | 0.4 | 3 | 03 | 4 | 3 |
| $\tau$(Ni II) | 0.8 | 0.8 | 3 | 4 | 3 |

Table 5. Fitting Parameters for Shallow–Silicon SNe Ia

| | SN 1999ee | SN 1999aw | SN 2000cx | SN 1991T | SN 2002cx |
|---|---|---|---|---|---|
| $v_{\rm phot}$ (km s$^{-1}$) | 11,000 | 13,000 | 13,000 | 11,000 | 6000 |
| $v_{\rm e}$ (km s$^{-1}$) | 1000 | 1000 | 1000 | 1000 | 1000 |
| $T_{\rm exc}$ (K) | 10,000 | 10,000 | 10,000 | 10,000 | 10,000 |
| $\tau$(O I) | 0.3(6)/12 | 0.3(6) | 0.5(6)/[25] | 0.4 | |
| $\tau$(Mg II) | 2 | 0.5(4) | 1.5 | 0 | 0.4 |
| $\tau$(Si II) | 4 | 1.5/15 | 3/15[16] | 0.4 | 0.6 |
| $\tau$(Si III) | 1 | 0.5 | 0.5/14 | 1.5 | 0.8 |
| $\tau$(S II) | 2 | 1.6 | 0.8/14 | 0.4 | 0.6 |
| $\tau$(Ca II) | 70 | 30 | 100 | 1.8 | 3 |
| $\tau$(HV Ca II) | 10(6)/19 | 8(6)/19 | 80/23 | 0.4(2)/20 | 0.5/14 |
| $\tau$(HV Sc II) | 0 | 0 | 0 | 0 | 0 |
| $\tau$(HV Ti II) | 0 | 0 | 1/23 | 0 | 0 |
| $\tau$(HV V II) | 0 | 0 | 4/23 | 0 | 0 |
| $\tau$(HV Cr II) | 0 | 0 | 1/22 | 0 | 0 |
| $\tau$(HV Fe II) | 0.6(4)/18 | 0.2(4)/18 | 0.8(5)/20 | 0.15(2)/19 | 0.4/13 |
| $\tau$(Fe III) | 0.8 | 0.8 | 0.8 | 0.9 | 0.8 |
| $\tau$(Co II) | 0.8 | 0.2 | 0 | 0 | 0 |
| $\tau$(Ni II) | 1.8 | 1.2 | 1.5 | 0 | 0.4 |